Batteries & Supercaps

Research Article
doi.org/10.1002/batt.202400630

Chemistry Europe
European Chemical Societies Publishing

www.batteries-supercaps.org

Wood-inspired High Ionic Conductivity Hydrogel Electrolytes for Flexible Supercapacitors

Chenxiang Gao,[c] Yue Liu,[a] Jiuzhou Zhang,[a] Hui Li,[b] Yang Liu,[a] Jiyou Gu,[a] Tianyi Ma,*[b] and Pengfei Huo*[a]

Hydrogel is a promising electrolyte substrate, but its ionic conductivity needs further improvement. In this paper, we propose a strategy to improve the ionic conductivity of hydrogels with flexible wood and fabricate a flexible wood-based poly(acrylic acid-acrylamide) composite hydrogel electrolyte (WHE) by delignification and in-situ polymerization. The flexible wood as a porous backbone for hydrogels can regulate ion transport pathways to improve the ionic conductivity of hydrogels. The straight pores of wood confine the transport of electrolyte ions along the shortest path, resulting in a high ionic conductivity of 3.0×10^{-2} S cm^{-1}, which is great in composite polymer electrolytes. We have systematically investigated the effect of the degree of delignification and the polymerization process on the overall performance of the electrolyte. The optimized supercapacitor exhibits a specific capacitance of 155.64 F g^{-1} and an energy density of 7.45 W h kg^{-1}. The WHE is applied to flexible supercapacitor, which exhibits good flexibility under bending conditions and can maintain similar electrochemical performance at a wide range of bending angles. This work provides an effective strategy for the efficient use of wood resources and the development of low-cost, environmentally friendly, and high-performance hydrogel electrolyte materials.

Introduction

In recent years, wearable electronic devices have developed rapidly, which requires the development of lightweight, mechanically flexible, biocompatible, safe, and reliable power materials with excellent performance.[1,2] Supercapacitor (SC) is a superior energy storage device with faster charge/discharge rates, higher capacitance, power density and longer cycle life.[3–5] It is a promising next-generation energy storage component. Qualified supercapacitors for wearable devices need to have not only ultra-high flexibility but also high energy density, high power density and cycling stability.[6]

The electrodes and electrolytes influence the performance of supercapacitors. The above needs can be met in two ways: by printing[7] or coating,[8] the conductive polymer is evenly distributed on the flexible substrate to produce high-performance electrodes; Alternatively, use a hydrogel electrolyte.[9,10] Currently, there are many reports for hydrogel electrolytes, but the dimensional stability of hydrogels is poor and hydrogels do not have a high enough ionic conductivity. Nowadays, much research is focused on the design and preparation of composite hydrogel electrolytes, which is indeed an effective strategy for improving the performance of hydrogels. Such as Lu et al.[11] prepared a nano-composite gel polymer electrolyte using Li^+ functionalized SPEEK nanofiber membrane as a substrate and composite PVA gel; Bae et al.[12] designed a 3D nanostructured hydrogel-derived LLTO backbone and composite PEO electrolyte to obtain a high-performance solid-state composite polymer electrolyte material. However, the ionic conduction pathways of the composite polymer electrolytes in these reports are uncontrollable and factors such as addition content have a serious impact on performing the electrolytes. Therefore, we use biomimetic principles to introduce flexible wood into hydrogels to construct composite polymer electrolytes with confined ion transport channels to improve ion transport efficiency, resulting in supercapacitors with even better performance.

It is well known that wood, as a natural renewable material, is extremely abundant and has characteristics such as lightweight, low thermal conductivity, high mechanical strength, and easy processing, making it one of the most sustainable, aesthetic and environmentally friendly materials.[13,14] Not only that, but wood is also a material with an extremely well-developed pore structure, with numerous large mesopores and a few micropores distributed within it, forming a unique hierarchical pore structure.[15–17] This unique structure not only plays a supporting role in trees but is also used to transport small molecules such as water, inorganic salts, and organic nutrients from the roots to the crown, and it is this special structure that makes wood a promising substrate material.[18] When wood is used as an electrolyte, the mesopores in the wood act as ion reservoirs, and the oriented channels with low tortuosity are enabled by the anisotropic structure, shortening the ion diffusion distance during charging and discharging.[19,20] The use of wood as a porous backbone for the preparation of wood-based composite hydrogel materials has been widely

[a] Y. Liu, J. Zhang, Y. Liu, J. Gu, P. Huo
Key Laboratory of Bio-based Material Science and Technology of Ministry of Education, Northeast Forestry University, Harbin 150040, China
E-mail: huopengfei@nefu.edu.cn

[b] H. Li, T. Ma
School of Science, RMIT University, Melbourne, VIC 3000, Australia
E-mail: tianyi.ma@rmit.edu.au

[c] C. Gao
School of Chemistry and Chemical Engineering, Northwestern Polytechnical University, Xi'an 710072, China

Supporting information for this article is available on the WWW under https://doi.org/10.1002/batt.202400630

Research Article
doi.org/10.1002/batt.202400630
Chemistry Europe
European Chemical Societies Publishing

used in sensors[21,22] and biomedical applications,[23] and these studies have shown that the wood backbone can indeed enhance the dimensional stability of hydrogels. However, there is a lack of reports on the analysis of flexible wood to improve the ionic conductivity of hydrogels, and there are few reports on the application of flexible wood-based composite hydrogel electrolytes in the field of flexible supercapacitors.

Here, we report on a wood-inspired approach to preparing flexible wood-based composite hydrogel electrolytes through a simple delignification treatment and in-situ polymerization reaction. Through a simple delignification treatment, we can impart good flexibility to the balsa wood, freeing it from the limitations of its brittleness. In addition, the regular arrangement of micro-pore channels inside the wood allows for efficient and fast transport of electrolyte ions, enabling WHEs to achieve ionic conductivity of over 3×10^{-2} S cm^{-1}, far exceeding that of comparable electrolyte materials. Meanwhile, we used WHEs combined with activated carbon electrodes to construct supercapacitors and tested their electrochemical performance under different conditions, finding that the specific capacitance of the supercapacitors could reach 155.64 F g^{-1} and the energy density up to 7.45 W h kg^{-1} at a current density of 0.2 A g^{-1}, demonstrating the great potential of wood as a substrate. We finally applied this composite hydrogel electrolyte to construct flexible supercapacitors that can be used over a wide range of bending angles and exhibit good flexibility by maintaining a capacitance retention of 90.51% after 180° bending for 100 times, which is beneficial for the development of wearable electronic devices.

Results and Discussion

Figure 1 briefly illustrates the preparation of wood hydrogel, comprising a continuous process of saw cutting, delignification and in-situ polymerization. Cutting in a direction perpendicular to the natural balsa wood growth results in a series of balsa wood slices, which are not well-flexible, breaking upon bending (Figure 1c, Video S1). As shown in Figure 1d, the delignification treatment not only removes some of the lignin and hemicellulose and softens the wood cell wall, but also exposes a large amount of cellulose.[24] The cellulose molecular chain contains many hydroxyl groups, which can form hydrogen bonds with the hydrogel to enhance the stability of material and generate complexation with lithium ions to improve ion transport efficiency.[25,26] After delignification, the flexibility of the balsa wood has been significantly improved and can be bent at large angles (Figure 1d, Video S2). Wood hydrogels prepared by in-situ polymerization retain the good flexibility of delignified wood and hydrogel and can be curled without breaking (Figure 1e), which is the basis for use in flexible supercapacitors.

As shown in Figure S1, a large weight loss in the wood occurred after only 1 h of treatment, with minimal subsequent weight loss. The results indicate that delignification removes organic components from the wood, but the longer treatment times have not a significant effect on the removal of these substances. The partial removal of lignin and hemicellulose was confirmed by comparing the FTIR spectra of the flexible wood. As shown in Figure S2, the correlation peaks for lignin are at 1596 cm^{-1}, 1506 cm^{-1} and 1454 cm^{-1}, originating from the aromatic skeleton vibrations,[27] while the correlation peaks for hemicellulose are at 1729 cm^{-1} and 1228 cm^{-1}, originated from the -(C=O)- and -(C=O)-O- vibrations on hemicellulose.[28] The spectra indicate that after delignification, some lignin and hemicellulose remain.

We measured the cell wall thickness given in the SEM images (shown in Figures 2a and b) by software (Nano Measurer 1.2.5). And 60 data points were obtained for each sample, they are shown in Table S1. The average thickness of cell walls changed from 2.12 μm to 0.82 μm, which indicated that after delignification, the cell walls become thinner. At a magnification of 500, the closely packed porous structure of the delignified wood can be observed (Figures S3 and S4), and the straight pores inside the wood can be observed. The straight internal pores of the wood have an excellent ability to regulate ion

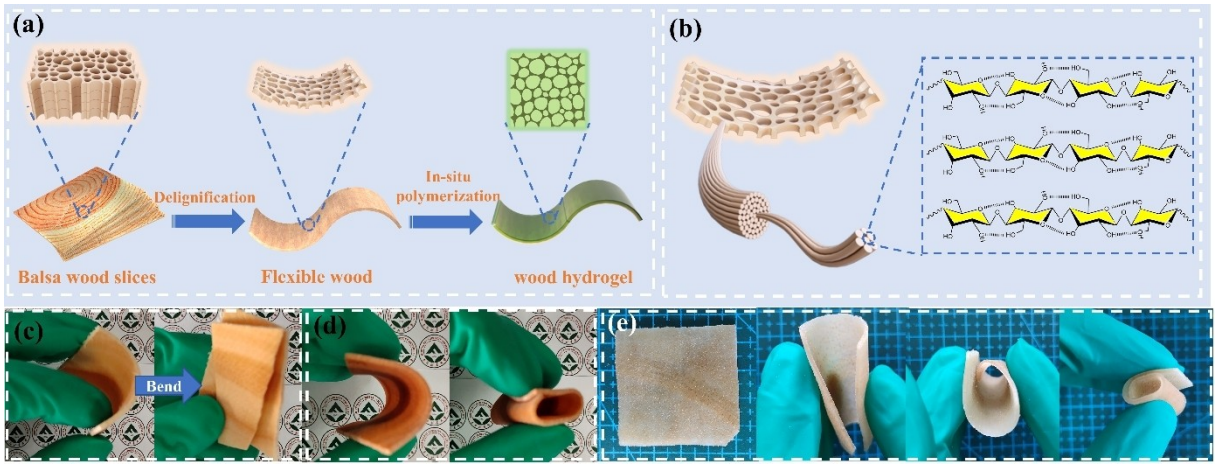

Figure 1. Diagrammatic sketch showing the design concept of wood hydrogel. (a) Fabrication procedure of wood hydrogel involving three steps of saw cutting, delignification and in-situ polymerization. (b) Schematic diagram of the microstructure of cellulose fibers in flexible wood. Photo images of (c) natural wood and (d) flexible wood before and after bending. (e) Diagram of the curling process of wood hydrogel.

Research Article
doi.org/10.1002/batt.202400630
Chemistry Europe
European Chemical Societies Publishing

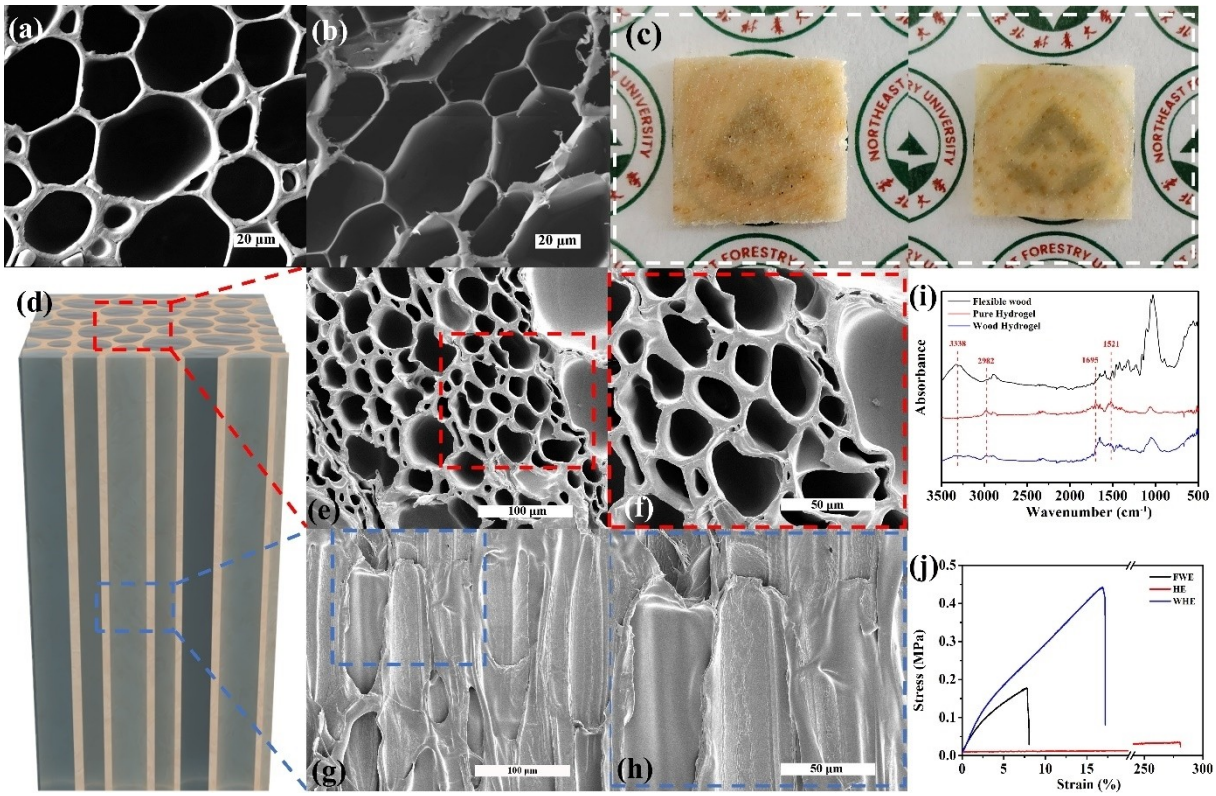

Figure 2. High magnification (a~b) images of natural wood and FW-6 cross section. (c) Electronic photos of FW-3 (left) and wood hydrogel (right). (d) Schematic diagram of the structure of the wood hydrogel. (e, f) Top-view SEM images of wood hydrogel. (g, h) Longitudinal SEM images of wood hydrogel. (i) FTIR spectra of the flexible wood, P(AA-co-AM) hydrogel and wood hydrogel. (j) Stress-strain curves of flexible wood electrolyte, P(AA-co-AM) hydrogel electrolyte and composite hydrogel electrolyte.

transport paths and are the source of the electrolyte's high ionic conductivity.

The FW-3 is chosen as the flexible substrate due to its mechanical properties (Figure S5) and economy. The P(AA-co-AM) hydrogel was homogeneously grown into the pores of the wood by the in-situ polymerization reaction to obtain a wood hydrogel which has excellent flexibility under varying degrees of bending (Video S3). During the in-situ polymerization reaction phase, thanks to the open and low tortuosity structure of the wood, the solution can easily penetrate the pores of the wood.[29] Figure 2c shows the electronic photos of FW-3 and wood hydrogel. From a macroscopic point of view, the larger pores and surfaces of the wood are filled with hydrogel after in-situ polymerization. From a microscopic point of view, the top-view SEM images demonstrate P(AA-co-AM) hydrogel on the surface of the flexible wood cell walls (Figures 2e and f). The longitudinal SEM images show the growth of P(AA-co-AM) hydrogel into the flexible wood pores (Figures 2g and h), the hydrogel uniformly grew on the straight pores of the wood. The directionally aligned pore structure of flexible wood allows for further regulation of ion transport paths and improved ionic conductivity. The distribution of P(AA-co-AM) hydrogel in the wood pores can also be clearly observed in the low magnification SEM images (Figure S6). Figure 2i shows the FTIR spectra of flexible wood, P(AA-co-AM) hydrogel and wood hydrogel. The peaks associated with P(AA-co-AM) hydrogel are at 2982 cm^{-1}, 1695 cm^{-1} and 1521 cm^{-1} from the stretching vibration of N–H, the stretching vibration of C=O of $CONH_2$, and the asymmetric stretching vibration of COO– respectively.[30] These three peaks are not observed on the FTIR spectra of flexible wood but can be observed on the FTIR spectra of P(AA-co-AM) hydrogel and wood hydrogel. 3338 cm^{-1} of the peak originates from the stretching vibration of O–H, which is not observed in the spectra of P(AA-co-AM) hydrogel but can be observed on the FTIR spectra of flexible wood and wood hydrogel. The peak is observed on the infrared spectra of the flexible wood and wood hydrogel. This indicates that the P(AA-co-AM) hydrogel is successfully grown into the flexible wood.

As shown in Figure 2j, the P(AA-co-AM) hydrogel electrolyte shows great deformation and very little strength; whereas the flexible wood electrolyte shows high strength and low deformation, and when the wood and hydrogel have finished compositing, the composite hydrogel electrolyte shows enhanced strength and suitable deformation. This shows the enhancing effect of wood on hydrogels. Hydrogels can be used for applications at large strains, but their strength is poor, while wood has high mechanical strength but low strain, each with certain limitations. Wood can effectively limit the swelling of hydrogel, after soaking in 1 M Li_2SO_4 for 24 h, the TSR and VSR of the wood hydrogel are only 13.39% and 30.04%, while that of P(AA-co-AM) hydrogel is 61.00% and 249.60%, which is a great difference (Figure S7). Using wood as a substrate and

compounding hydrogel materials, it prepared the wood hydrogel with both high tensile strength and large strain, making it a promising electrolyte material.

As shown in Figure 3a, the pores of wood can transport the water and inorganic salts to the various parts of the plant, this structure of wood is naturally efficient in transporting ions. After delignification and compound of hydrogel, the straight pore structure of the wood is perfectly preserved and the electrolyte ions can be transported along the shortest possible path. It is fundamental to the high ionic conductivity of composite hydrogel electrolytes and guarantees the excellent performance of supercapacitors. Compared to flexible wood electrolyte and P(AA-co-AM) hydrogel electrolyte, the ionic conductivity of composite hydrogel electrolyte is significantly improved (3.0×10^{-2} S cm^{-1}), because of the combination of the wood's ability to transport electrolyte ions rapidly and the hydrogel's ability to absorb electrolyte ions effectively (Figure 3b). At the same time, the electrolyte prepared in this paper shows considerable advantages in comparison with the ionic conductivity of similar electrolytes (Figure 3c).

The WHSCs consisted mainly of composite hydrogel electrolytes, AC electrodes and current collectors (Figure 3d). The composite hydrogel electrolyte has a thickness of 0.8~1.1 mm. The mass loading of AC active material is 4 mg. We discussed the effect of different experimental parameters (see Tables S2–S4 for details) on performing the products. Figures 3e–g show the effect of different experimental parameters on the specific capacitances of supercapacitors. As shown in Figure 3e, when the molar ratio of AA–AM is 0.1:1, the highest specific capacitance occurs and the device performs best. Other test results show that the ionic conductivity and mechanical strength of the WHE-0.1:1 are greatest currently and that the device has the highest energy density and power density (Figures S8 and S9). As the ratio of AA to AM increases, the performance of the material decreases, possibly because the proportion of –COO– in the reaction solution increases and the intermolecular repulsion strengthens, blocking the polymerization reaction. At a cross-linker content of 0.2 mol% of AM, the WHE-0.2% MBA shows the maximum ionic conductivity and strain (Figure S10 and Figure S11). At this point, the supercapacitor performs at its best, exhibiting the highest specific capacitance (Figure 3f). As the cross-linker content increases, the electrochemical performance of the material shows a decreasing trend. The reason for this is that crosslinking is too

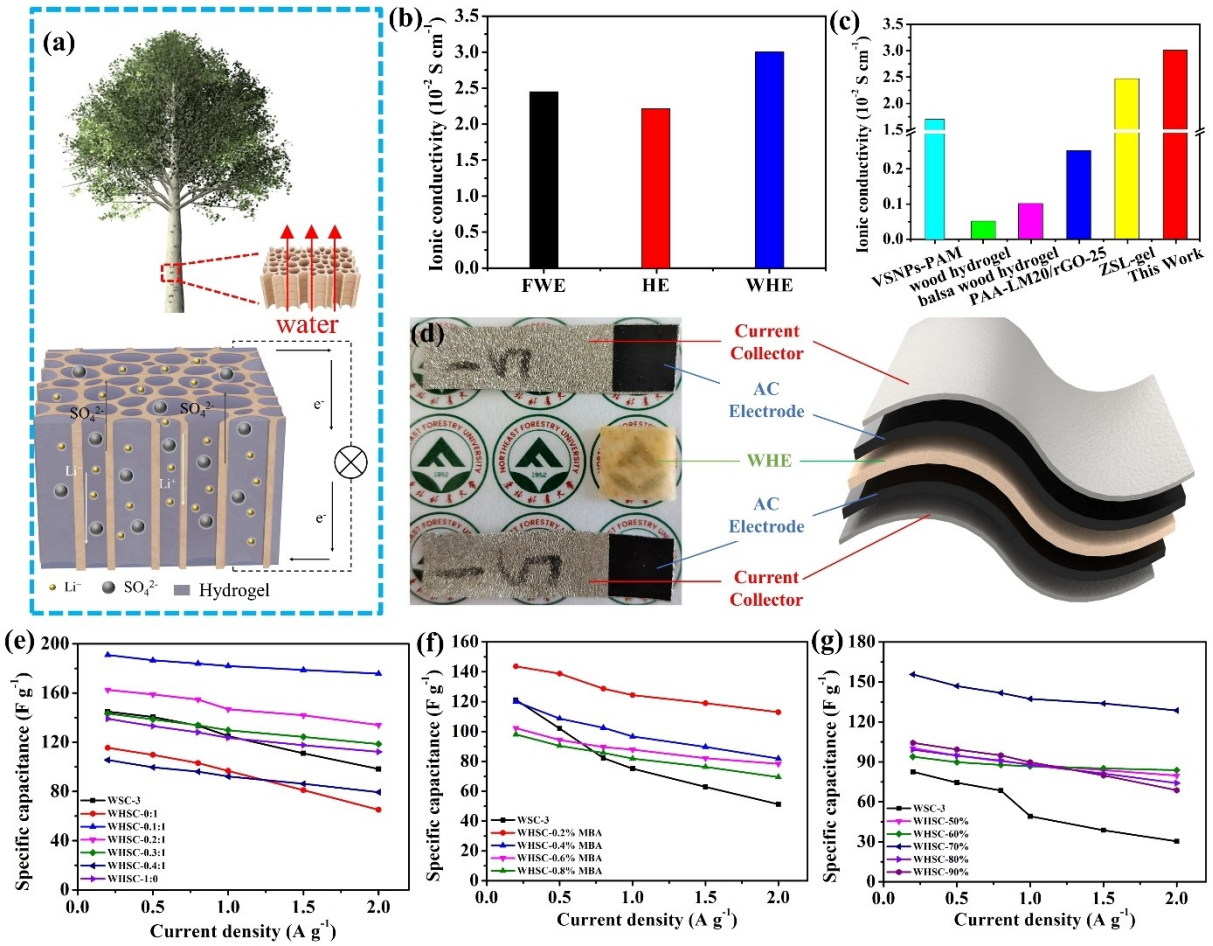

Figure 3. Diagram of the transport of (a) water molecules by wood and electrolyte ions by composite hydrogel electrolyte. (b) Ionic conductivities of flexible wood electrolyte, P(AA-co-AM) hydrogel electrolyte and composite hydrogel electrolyte. (c) Ionic conductivity of flexible wood electrolytes compared with other reported similar electrolytes (VSNPs-PAM,[31] wood hydrogel,[32] balsa wood hydrogel,[33] PAA-LM20/rGO-25,[34] ZSL-gel[35]). (d) Schematic diagram of the WHSC structure. The effect of (e) the ratio of AA to AM, (f) cross-linker content and (g) AA neutrality on the specific capacitances of supercapacitors.

Research Article
doi.org/10.1002/batt.202400630
Chemistry Europe
European Chemical Societies Publishing

high, which is not conducive to the transport of electrolyte ions. Figure 3g shows that the supercapacitor exhibits the highest specific capacitance when the AA neutrality is 70%. Figure S12 and Figure S13 show that WHE-70% has the highest ionic conductivity, tensile strength, and strain. At this point, the device shows the best performance. At lower neutralization levels, the amount of –COO– is low, which is not conducive to complexation with Li+ and makes the material less efficient for ion transport, while at higher neutralization levels, the amount of –COO– is high and intermolecular repulsion is strong, which is not conducive to polymerization reactions, hence the need to choose a suitable neutralization level. In summary, when the molar ratio of AA–AM is 0.1:1, the cross-linker content is 0.2 mol% of AM, and the AA neutrality is 70%, the best performance of the prepared wood hydrogel is achieved, and the resulting constructed supercapacitor is named WHSC-BEST.

Figure 4 shows the electrochemical performance of WHSC-BEST. As shown in Figure 4a and Video S4, when connected to an LED lamp circuit, WHSC-BEST can light up the LED lamp and keep it powered for 4 min. In addition, the WHSC-BEST could drive a windmill (Video S5). The EIS plots show a tiny semicircular in the high frequency region, indicating a good interface between the composite hydrogel electrode and AC electrolytes, and the phase angle of almost 80° indicates a good capacitive behavior of WHSC-BEST (Figure 4b). The symmetrical rectangular shape of the CV curves at scan rates from 10 to 150 mV s^{-1} in Figure 4c and the isosceles triangular shape of the GCD profiles at different current densities in Figure 4d demonstrates the excellent electrochemical performance of WHSC-BEST. As shown in Figure S14, WHSC-BEST can operate stably at a wide voltage range. As shown in Figure 4e, at the current density of 0.2 A g^{-1}, the supercapacitor's energy density can be up to 7.45 W h kg^{-1}, demonstrating a performance that exceeds that of similar devices. Figures 4f and g show the CV curves and the GCD profiles for two supercapacitors connected in series and parallel, respectively. The change pattern of CV curves GCD profiles is under the basic rules for series and parallel connections.[36,37] To investigate the cycling stability of WHSC-BEST, we carried out 3000 cycles at a current density of 1.0 A g^{-1}. Thanks to the wood substrate, WHSC-BEST obtained good stability, with a cycle retention rate of 88.32% after 3000 cycles (Figure 4h), much higher than the 71.4% of flexible wood electrolyte-based supercapacitor. In addition, the high Coulombe efficiency of 99.56% demonstrates the good reversibility

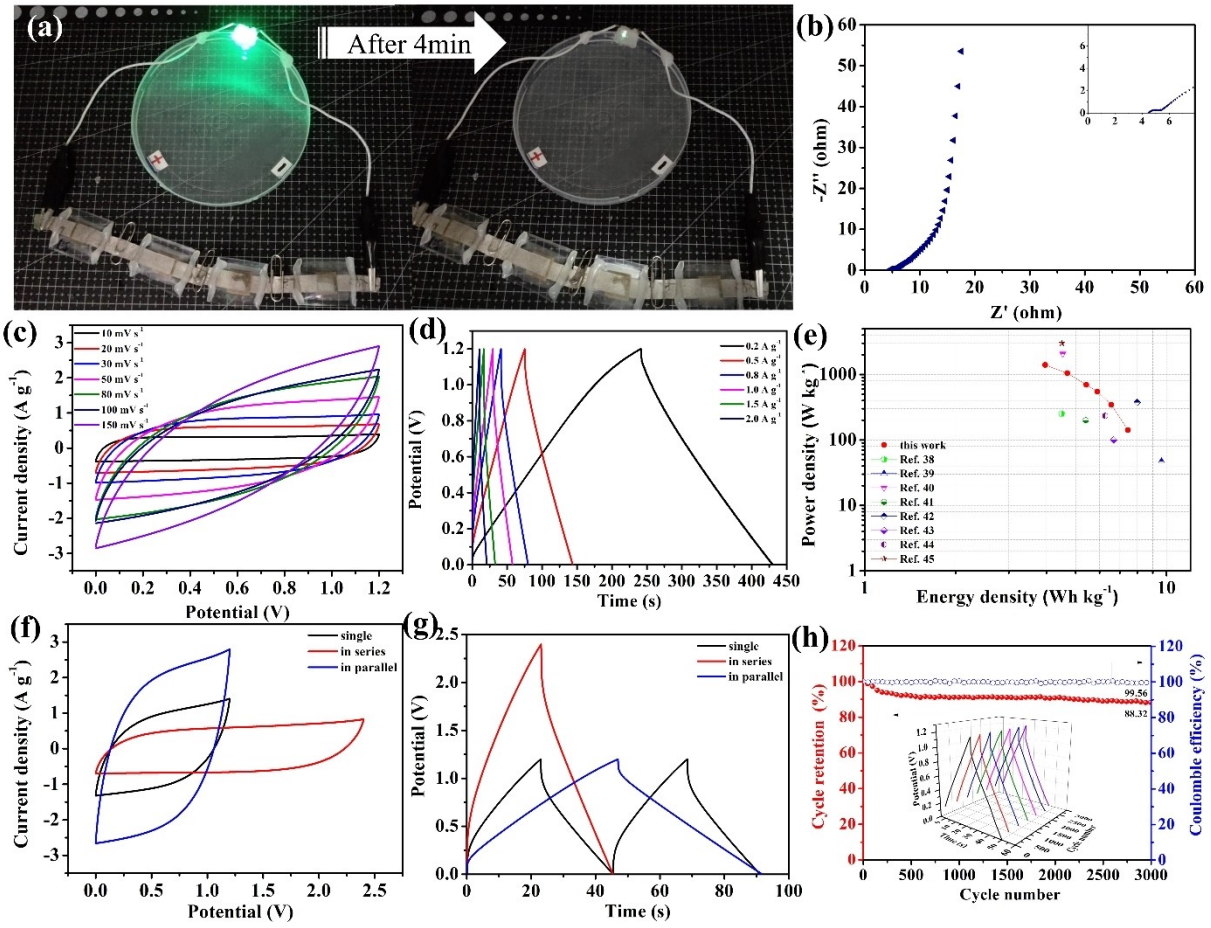

Figure 4. Electrochemical performance of WHSC-BEST. (a) Photo image of the driving LED lamp. It can be powered continuously for 4 min. (b) EIS plots of WHSC-BEST. Inset: local magnification. (c) CV curves of WHSC-BEST at different scan rates. (d) GCD profiles of WHSC-BEST at different current densities. (e) Ragone plots of the WHSC-BEST and performance comparison with previously reported biomass-based supercapacitor.[38–45] (f) CV curves and (g) GCD profiles of a single and two WHSC-BEST connected in series and parallel. (h) Capacitance stability of WHSC-BEST at a current density of 1.0 A g^{-1}. Inset: GCD profiles every 500 cycles.

Research Article
doi.org/10.1002/batt.202400630
Chemistry Europe
European Chemical Societies Publishing

of WHSC-BEST for charging and discharging. No significant fluctuations are observed in the GCD profiles at 500 cycle intervals, further demonstrating the excellent cycle stability of the supercapacitor. The synergy between the flexible wood as a substrate, which ensures efficient transport of electrolyte ions, and the large number of reactive groups in the P(AA-co-AM) hydrogel, which gives the electrolyte excellent storage capacity for electrolyte ions, gives the supercapacitor excellent electrochemical performance.

Flexibility is the key to achieving wearable devices. To further investigate the flexibility of WHSC-BEST, the electrochemical performance of the supercapacitor for bending degrees of 0°, 45°, 90°, 135° and 180° was tested, as shown in Figure 5. The device can supply stable power to an LED lamp in both the original and bending states (Figure 5a, Video S6). Also, the EIS plots, CV curves and GCD profiles shown in Figures 5b–d show almost overlap, which further illustrates the excellent flexibility of the supercapacitor. Compared with other reported flexible supercapacitors, WHSC-BEST has certain advantages, the capacitance retention could reach 90.51% after 100 bends at 180° (Figure 5e) resulting from the good stability given by the flexible wood substrate. The excellent flexibility of the flexible wood and P(AA-co-AM) hydrogel, allows the wood hydrogel to keep its good flexibility while achieving better electrochemical performance, providing an idea for the development of flexible supercapacitors.

Figure S15 shows the electrochemical performance of flexible wood electrolyte-based supercapacitors. The fitted results of the equivalent circuit show that the equivalent series resistance (Rs) of WSC-0 is as high as 9.96 Ω, while the Rs of the other WSCs is only around 2 Ω (Figure S16), indicating that the internal resistance of the device is significantly reduced after delignification. In conclusion, the electrochemical performance of wood after delignification treatment was significantly improved, WSC-3 has the best overall performance and its electrochemical performance is shown in Figure S17.

Figure 6a shows the discharge and charge of WHSC, the electrolyte ions are transported along the ion channels of the flexible wood. The flexible wood acts as a backbone for the composite hydrogel electrolyte, providing ion channels that not only store electrolyte ions, but are also the shortest path for electrolyte ion transport. Figures 6b–e compare the electrochemical performance of supercapacitors based on flexible wood electrolyte, P(AA-co-AM) hydrogel electrolyte, and composite hydrogel electrolyte, respectively. Because of the ultra-high-water content within the hydrogel, HSC exhibits a small equivalent series resistance, but the large semicircle in the high frequency region and phase angle of around 60° in the low frequency region indicate its poor interfacial and capacitive behavior (Figure 6b). As shown in Figures 6c and d, the CV curves of WHSC show a larger integration area and a near-rectangular shape, and the GCD profiles have an isosceles triangle shape, showing longer charge/discharge times and smaller voltage drop. The excellent synergistic effect between flexible wood and P(AA-co-AM) hydrogel further promoted the electrochemical performance of the supercapacitor. The specific capacitance of WSC, HSC and WHSC at different current densities (Figure 6e) showed results consistent with the above analysis, further confirming that the wood hydrogel possesses excellent capacitive behavior.

Overall, flexible wood plays a crucial role in flexible wood-based hydrogel polymer electrolytes for promoting the electrochemical performance of the supercapacitors: (1) The well-developed pore structure of wood confines ion channels and shortens the ion transport path of flexible wood-based composite hydrogen polymer electrolyte. (2) The flexible wood

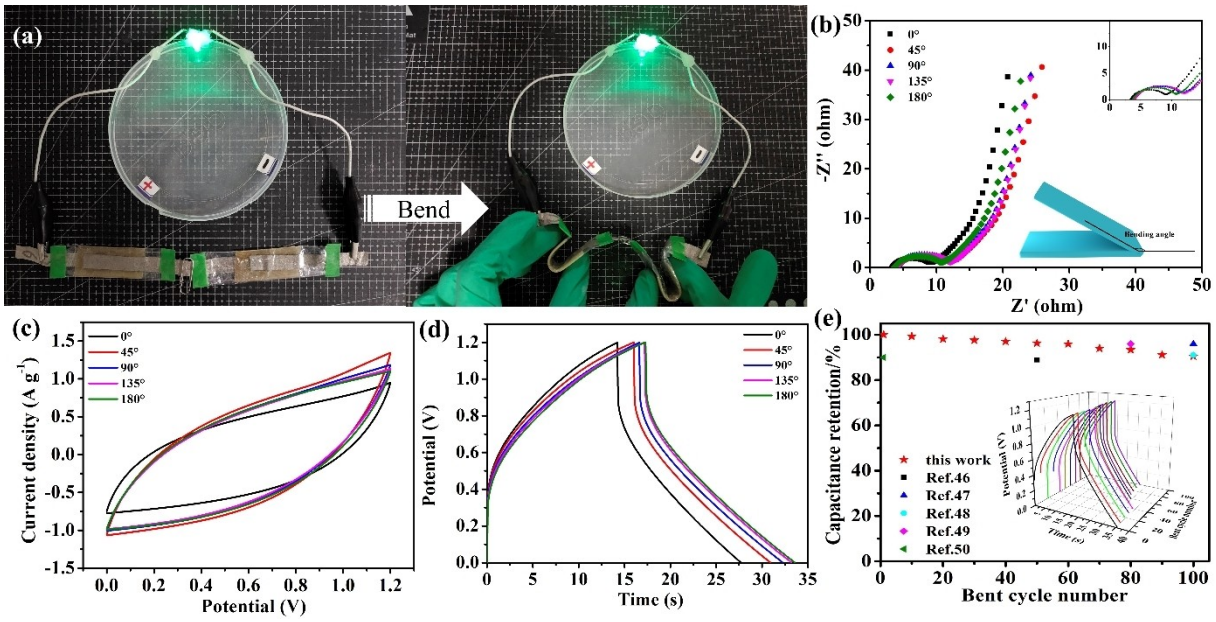

Figure 5. Bending performance of WHSC-BEST. (a) Photo image of the driving LED lamp in original state (left) and bending state (right). (b) EIS plots (insets show bending angle and local magnification) (c) CV curves and (d) GCD profiles of WHSC-BEST under different bending angles. (e) Capacitance stability of WHSC-BEST bent 180° for 100 cycles. Inset: GCD profiles every 10 cycles.[46–50]

Research Article
doi.org/10.1002/batt.202400630
Chemistry Europe
European Chemical Societies Publishing

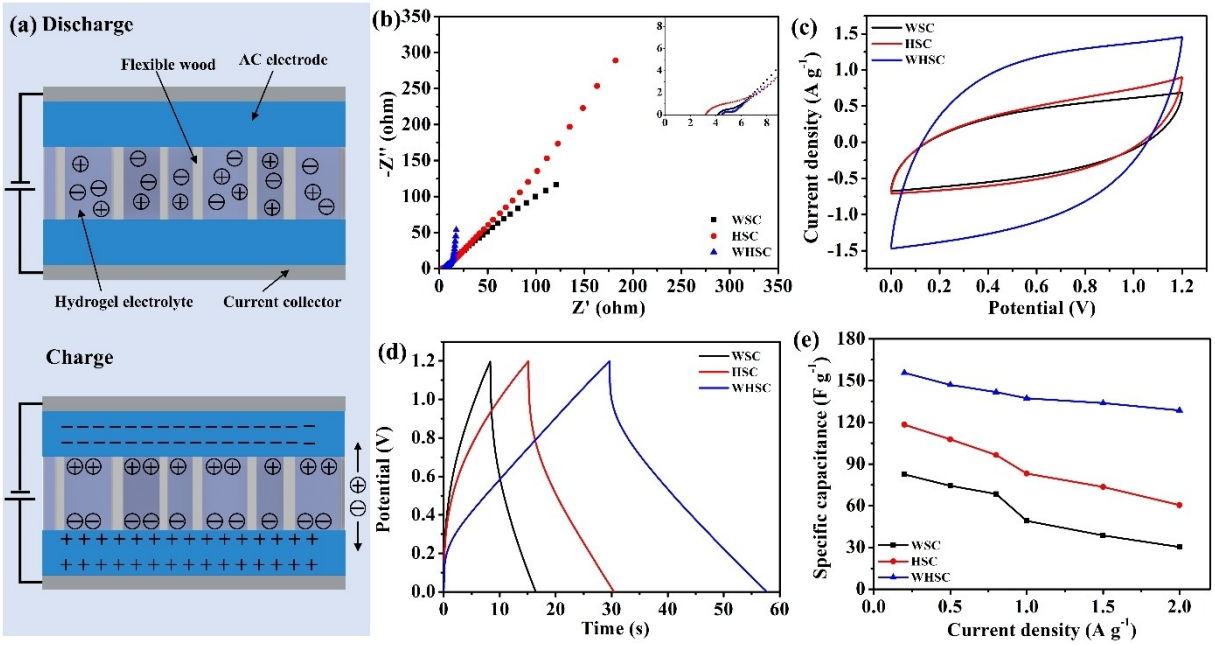

Figure 6. (a) The discharge and charge of WHSC. Electrochemical performance of WSC, HSC and WHSC: (b) EIS plots (c) CV curves and (d) GCD profiles of WSC, HSC and WHSC. (e) Specific capacitances of WSC, HSC and WHSC as a function of current density.

prevents excessive swelling of hydrogels to provide excellent dimensional stability and mechanical properties. (3) The biomimetic composite hydrogel optimizes the electrochemical performance of supercapacitors by the synergistic effect of flexible wood and hydrogel.

Conclusions

In summary, flexible wood/P(AA-co-AM) hydrogel electrolyte materials were successfully prepared by obtaining flexible wood substrates through a simple delignification treatment and in-situ polymerization. Because of the regulation effect of the straight pores of wood on the ion transport path, the composite hydrogel electrolyte exhibits a high ionic conductivity (3.0×10^{-2} S cm^{-1}). And the addition of P(AA-co-AM) hydrogel enables the wood hydrogel to absorb electrolyte ions effectively and obtain excellent capacitive behavior. The electrochemical performance of supercapacitors constructed using wood hydrogels is superior to that of supercapacitors constructed from flexible wood and P(AA-co-AM) hydrogels. The optimal ratios are obtained when the molar ratio of AA to AM is 0.1 : 1, the cross-linker content is 0.2 %, and the AA neutralization is 70 %. The supercapacitor exhibits the highest specific capacitance (155.64 F g^{-1}), and the highest energy density (7.45 W h kg^{-1}). Bending tests show that the supercapacitor constructed from wood hydrogel has good flexibility. Therefore, the wood hydrogel shown here is a promising candidate for an efficient electrolyte material for energy storage devices.

Supporting Information Summary

Experimental Section: Materials and Chemicals; Preparation of Flexible Wood; Preparation of the composite hydrogel electrolyte; Preparation of the AC Electrodes; Fabrication of Supercapacitors; Characterization of Materials; Electrochemical Characterization of Supercapacitors. Change in weight retention of wood samples with delignification time; SEM images and FTIR spectra of the natural wood and flexible wood; Mechanical performance of FWEs; SEM images of wood hydrogel; Photos of wood hydrogel and P(AA-co-AM) hydrogel before and after 24 hours of immersion in 1 M Li2SO4; The effect of the ratio of AA to AM, cross-linker and neutralization on electrochemical performance and mechanical performance; Linear sweep voltammetry profile of WHSC-BEST; Electrochemical performance of WSCs and WSC-3; Four tables respectively record cell wall thickness of the balsa wood before and after delignification and experimental parameters (molar ratio of AA–AM, cross-linker content, neutralization). Video S1: Bending of the natural balsa wood (MP4); Video S2: Bending of the FW-3 (MP4); Video S3: Bending of the wood hydrogel (MP4); Video S4: Supercapacitors driven a LED lamp (MP4); Video S5: Supercapacitors powering a windmill (MP4); Video S6: Supercapacitors powering a LED lamp in a bent state (MP4).

Acronyms

HE	Poly(acrylic acid-acrylamide) hydrogel electrolyte
WHE	Wood hydrogel composite electrolyte
FEW	Flexible wood electrolyte
SC	Supercapacitor

FW-n, n is delignification time	Flexible wood
WHSC	The supercapacitors with WHE
WSC	The supercapacitors with flexible wood electrolytes
HSC	The supercapacitors with P(AA-co-AM) hydrogel electrolytes

Acknowledgements

This work was supported by the Fundamental Research Funds for the Central Universities [2572021BB08], China Postdoctoral Science Foundation [2017M621230].

Conflict of Interests

The authors declare no conflict of interest.

Data Availability Statement

Research data are not shared.

Keywords: Wood hydrogel · Composite polymer electrolyte · Flexible supercapacitor · High ionic conductivity

[1] W. Liu, M.-S. Song, B. Kong, Y. Cui, *Adv. Mater.* **2017**, *29*, 1603436.
[2] W. Qiu, Y. Tian, Z. Lin, S. Lin, Z. Geng, K. Huang, A. Lei, F. Huang, H. Feng, F. Ding, Y. Li, X. Lu, *J. Energy Chem.* **2022**, *70*, 283–291.
[3] E. Cevik, A. Bozkurt, *J. Energy Chem.* **2021**, *55*, 145–153.
[4] J. Liu, Z. Khanam, S. Ahmed, H. Wang, T. Wang, S. Song, *J. Power Sources* **2021**, *488*, 229461.
[5] N. Anjum, N. Joyal, J. Iroegbu, D. Li, C. Shen, *J. Power Sources* **2021**, *499*, 229962.
[6] Y. Ko, M. Kwon, W. K. Bae, B. Lee, S. W. Lee, J. Cho, *Nat. Commun.* **2017**, *8*, 536.
[7] A. D. Valentine, T. A. Busbee, J. W. Boley, J. R. Raney, A. Chortos, A. Kotikian, J. D. Berrigan, M. F. Durstock, J. A. Lewis, *Adv. Mater.* **2017**, *29*, 1703817.
[8] Y. Zhou, X. Wang, L. Acauan, E. Kalfon-Cohen, X. Ni, Y. Stein, K. K. Gleason, B. L. Wardle, *Adv. Mater.* **2019**, *31*, 1901916.
[9] R. Na, X. Wang, N. Lu, G. Huo, H. Lin, G. Wang, *Electrochim. Acta* **2018**, *274*, 316–325.
[10] M. Chen, M. Yang, X. Han, J. Chen, P. Zhang, C.-P. Wong, *Adv. Mater.* **2024**, *36*, 2304997.
[11] N. Lu, X. Zhang, R. Na, W. Ma, C. Zhang, Y. Luo, Y. Mu, S. Zhang, G. Wang, *J. Colloid Interface Sci.* **2019**, *534*, 672–682.
[12] J. Bae, Y. Li, J. Zhang, X. Zhou, F. Zhao, Y. Shi, J. B. Goodenough, G. Yu, *Angew. Chem. Int. Ed. Engl.* **2018**, *57*, 2096–2100.
[13] D. Li, D. Han, C. Guo, C. Huang, *ACS Appl. Energy Mater.* **2021**, *4*, 1752–1762.
[14] L. Li, R. Xiao, X. Tao, Y. Wu, L. Jiang, Z. Zhang, Y. Qing, *J. Power Sources* **2021**, *491*, 229618.
[15] C. Chen, L. Hu, *Acc. Chem. Res.* **2018**, *51*, 3154–3165.
[16] L. Li, Z. Chen, J. Lu, M. Wei, Y. Huang, P. Jiang, *ACS Omega* **2021**, *6*, 3921–3930.
[17] C. Chen, Y. Kuang, S. Zhu, I. Burgert, T. Keplinger, A. Gong, T. Li, L. Berglund, S. J. Eichhorn, L. Hu, *Nat. Rev. Mater.* **2020**, *5*, 642–666.
[18] M. Höglund, J. Garemark, M. Nero, T. Willhammar, S. Popov, L. A. Berglund, *Chem. Mater.* **2021**, *33*, 3736–3745.
[19] D. Yang, Y. Song, M.-Y. Zhang, Z. Qin, R. Dong, C. Li, X.-X. Liu, *Adv. Funct. Mater.* **2021**, *31*, 2100477.
[20] J. Chen, M. Chen, H. Chen, M. Yang, X. Han, D. Ma, P. Zhang, C.-P. Wong, *PNAS* **2024**, *121*, e2322944121.
[21] K. Nie, Z. Wang, R. Tang, L. Zheng, C. Li, X. Shen, Q. Sun, *ACS Appl. Mater. Interfaces* **2020**, *12*, 43024–43031.
[22] C. Chen, Y. Wang, T. Zhou, Z. Wan, Q. Yang, Z. Xu, D. Li, Y. Jin, *Biomacromolecules* **2021**, *22*, 5204–5213.
[23] X. Wang, J. Fang, W. Zhu, C. Zhong, D. Ye, M. Zhu, X. Lu, Y. Zhao, F. Ren, *Adv. Funct. Mater.* **2021**, *31*, 2010068.
[24] C. Chen, J. Song, J. Cheng, Z. Pang, W. Gan, G. Chen, Y. Kuang, H. Huang, U. Ray, T. Li, L. Hu, *ACS Nano* **2020**, *14*, 16723–16734.
[25] X. Zhang, X. Ma, T. Hou, K. Guo, J. Yin, Z. Wang, L. Shu, M. He, J. Yao, *Angew. Chem. Int. Edit.* **2019**, *58*, 7366–7370.
[26] J. Li, Z. Hu, S. Zhang, H. Zhang, S. Guo, G. Zhong, Y. Qiao, Z. Peng, Y. Li, S. Chen, G. Chen, A. Cao, *Nat. Sustain.* **2024**.
[27] H. Guan, Z. Cheng, X. Wang, *ACS Nano* **2018**, *12*, 10365–10373.
[28] J. Song, C. Chen, C. Wang, Y. Kuang, Y. Li, F. Jiang, Y. Li, E. Hitz, Y. Zhang, B. Liu, A. Gong, H. Bian, J. Y. Zhu, J. Zhang, J. Li, L. Hu, *ACS Appl. Mater. Interfaces* **2017**, *9*, 23520–23527.
[29] Y. Li, T. Gao, Y. Yao, Z. Liu, Y. Kuang, C. Chen, J. Song, S. Xu, E. M. Hitz, B. Liu, R. J. Jacob, M. R. Zachariah, G. Wang, L. Hu, *Adv. Energy Mater.* **2018**, *8*, 1801289.
[30] J. Zhang, A. Li, A. Wang, *React. Funct. Polym.* **2006**, *66*, 747–756.
[31] Y. Huang, M. Zhong, F. Shi, X. Liu, Z. Tang, Y. Wang, Y. Huang, H. Hou, X. Xie, C. Zhi, *Angew. Chem. Int. Ed. Engl.* **2017**, *56*, 9141–9145.
[32] W. Kong, C. Wang, C. Jia, Y. Kuang, G. Pastel, C. Chen, G. Chen, S. He, H. Huang, J. Zhang, S. Wang, L. Hu, *Adv. Mater.* **2018**, *30*, 1801934.
[33] G. Chen, T. Li, C. Chen, W. Kong, M. Jiao, B. Jiang, Q. Xia, Z. Liang, Y. Liu, S. He, L. Hu, *ACS Nano* **2021**, *15*, 11244–11252.
[34] Z. Zhang, L. Tang, C. Chen, H. Yu, H. Bai, L. Wang, M. Qin, Y. Feng, W. Feng, *J. Mater. Chem. A* **2021**, *9*, 875–883.
[35] F. Mo, Z. Chen, G. Liang, D. Wang, Y. Zhao, H. Li, B. Dong, C. Zhi, *Adv. Energy Mater.* **2020**, *10*, 2000035.
[36] Z. Yang, Y. Jia, Y. Niu, Y. Zhang, C. Zhang, P. Li, M. Zhu, Q. Li, *J. Energy Chem.* **2020**, *51*, 434–441.
[37] J. Yan, Y. Ma, C. Zhang, X. Li, W. Liu, X. Yao, S. Yao, S. Luo, *RSC Adv.* **2018**, *8*, 39742–39748.
[38] J. H. Park, H. H. Rana, J. Y. Lee, H. S. Park, *J. Mater. Chem. A* **2019**, *7*, 16962–16968.
[39] M. Wu, S. Xu, X. Li, T. Zhang, Z. Lv, Z. Li, X. Li, *J. Energy Storage* **2021**, *40*, 102663.
[40] S. Ahmed, A. Ahmed, M. Rafat, *J Energy Storage* **2019**, *26*, 100988.
[41] Z. Hu, S. Li, P. Cheng, W. Yu, R. Li, X. Shao, W. Lin, D. Yuan, *J. Mater. Sci.* **2016**, *51*, 2627–2633.
[42] G. A. Yakaboylu, C. Jiang, T. Yumak, J. W. Zondlo, J. Wang, E. M. Sabolsky, *Renew. Energ.* **2021**, *163*, 276–287.
[43] Y. Gong, D. Li, C. Luo, Q. Fu, C. Pan, *Green Chem.* **2017**, *19*, 4132–4140.
[44] S. Sarkar, A. Arya, U. K. Gaur, A. Gaur, *Biomass Bioenerg.* **2020**, *142*, 105730.
[45] M. Vinayagam, R. Suresh Babu, A. Sivasamy, A. L. F. de Barros, *Carbon Lett.* **2021**, *31*, 1133–1143.
[46] M. Zhang, J. Zhou, J. Yu, L. Shi, M. Ji, H. Liu, D. Li, C. Zhu, J. Xu, *Chem. Eng. J.* **2020**, *387*, 123170.
[47] J. Yu, J. Zhou, P. Yao, J. Huang, W. Sun, C. Zhu, J. Xu, *J. Power Sources* **2019**, *440*, 227150.
[48] P. He, Z. Ding, X. Zhao, J. Liu, Q. Huang, J. Peng, L.-Z. Fan, *Carbon* **2019**, *155*, 453–461.
[49] L. Liu, B. Shen, D. Jiang, R. Guo, L. Kong, X. Yan, *Adv. Energy Mater.* **2016**, *6*, 1600763.
[50] X. Li, H. Li, X. Fan, X. Shi, J. Liang, *Adv. Energy Mater.* **2020**, *10*, 1903794.

Manuscript received: September 25, 2024
Revised manuscript received: October 22, 2024
Accepted manuscript online: November 4, 2024
Version of record online: November 19, 2024